Experimental studies of zonal flow and field in compact helical system plasma[a)]

A. Fujisawa,[1,b)] K. Itoh,[1] A. Shimizu,[1] H. Nakano,[1] S. Ohshima,[1] H. Iguchi,[1] K. Matsuoka,[1] S. Okamura,[1] T. Minami,[1] Y. Yoshimura,[1] K. Nagaoka,[1] K. Ida,[1] K. Toi,[1] C. Takahashi,[1] M. Kojima,[1] S. Nishimura,[1] M. Isobe,[1] C. Suzuki,[1] T. Akiyama,[1] T. Ido,[1] Y. Nagashima,[2] S.-I. Itoh,[2] and P. H. Diamond[3]
[1]*National Institute for Fusion Science, Oroshi-cho, Toki-shi, 509-52 Japan*
[2]*RIAM, Kyushu University, Kasuga 816-8580 Japan*
[3]*University of California, San Diego, La Jolla, California 92093-0319, USA*

(Received 8 November 2007; accepted 5 February 2008; published online 12 March 2008)

The experimental studies on zonal flows and turbulence have been carried out in Compact Helical System [K. Matsuoka, S. Kubo, M. Hosokawa *et al.*, in *Plasma Physics and Controlled Nuclear Fusion Research, Proc. 12th Int. Conf.*, Nice, 1988 (International Atomic Energy Agency, Vienna, 1989, Vol. 2, p. 411] using twin heavy ion beam probes. The paper presents the experimental observations of stationary zonal flow, nonlinear couplings between zonal flow and turbulence, and the role of zonal flow in the improved confinement, together with the recent discovery of zonal magnetic field. The presented experimental results strongly support the new paradigm that the plasma transport should be considered as a system of drift wave and zonal flows, and provides the first direct evidence for turbulence dynamo that the structured magnetic field can be really generated by turbulence. © *2008 American Institute of Physics*. [DOI: 10.1063/1.2889012]

I. INTRODUCTION

A number of structures can be found to be associated with turbulence in the universe and nature. The examples include historical problems such as the geomagnetism, Jovian belts, transport in accretion disks, and so on. It has been known that the Jovian belts or zonal flows should be generated by the Rossby wave turbulence.[1] In 1970s, it was pointed out that the drift wave turbulence should obey the same equation as the Rossby wave turbulence,[2] therefore, it is expected that the zonal flows should exist in toroidal plasmas.

In fusion research, the importance of the zonal flows for the plasma confinement has been recognized and widely discussed for the precise prediction of the performance of the next generation device aiming at plasma burning. The drift wave turbulence governs the transport processes in toroidal plasmas, and the saturation level of the drift wave turbulence should be determined by the interaction between zonal flows and drift waves.

In toroidal plasmas, two kinds of zonal flows are expected to exist.[3] One is called stationary zonal flow, which is characterized by nearly zero frequency, and the other is geodesic acoustic modes (GAMs), an oscillatory branch of zonal flows. The zonal flows are symmetric around the magnetic field axis, i.e., $m=n=0$, and have a finite radial wavelength in mesoscale, i.e., $\lambda_r \sim \sqrt{\rho_i a}$, where a and ρ_i are the device size and the typical ion Larmor radius, respectively. The zonal flows are linearly stable; therefore, they are driven by the background turbulence nonlinearly.

After theoretical and simulation works suggested the existence of zonal flows and their roles in transport,[4–9] the existence of zonal flows was experimentally proven in a number of experiments;[10–13] more results are available for GAMs,[14–22] (for a review, see Ref. 23). The first complete identification of the stationary zonal flow was made in Compact Helical System (CHS) using twin heavy ion beam probes (HIBPs),[10] with the observation of coherent modes conjectured as GAMs.[21] Further progress has been made in CHS; for example, to really confirm the presence of the interaction or nonlinear coupling between zonal flow and turbulence[21,24–26] using an advanced data-processing technique—wavelet bicoherence analysis.

Moreover, we have developed a potential ability of the HIBP, which means the direct measurement of magnetic field fluctuations of plasma interior from the horizontal beam movement, and successfully obtained a spectrum of magnetic field fluctuations in CHS plasmas.[27] The paper presents a brief review of the experimental achievements, using twin HIBPs in CHS, on the system of zonal flows and turbulence, together with the discovery of the zonal magnetic field.[28] The discovery is, to the authors' knowledge, the first evidence to show that the turbulence really generates the structured magnetic field, which is associated with a historical physics problem; i.e., the dynamo problem.

II. EXPERIMENTAL SETUP

A. CHS device

CHS is a toroidal helical device, the major and average minor radii of which are $R=1$ m and $a=0.2$ m, respectively. The magnetic field of CHS is generated with a pair of helical coils and four pairs of poloidal coils to alter the properties of magnetic field configuration, such as magnetic well depth, helical ripples, rotational transform, and so on. CHS has sev-

[a)]Paper NI1 1, Bull. Am. Phys. Soc. **52**, 186 (2007).
[b)]Invited speaker.

eral heating apparatuses, two neutral beam injection systems and gyrotrons, to cover a wide range of plasma parameter regimes.

B. HIBP for zonal flow physics

The device is equipped with two HIBPs, located 90° apart in toroidal direction, in order to investigate global characteristics of plasma turbulence measured in electrostatic potential, density, and their fluctuations simultaneously. Each HIBP has three channels to observe the adjacent spatial points to examine the local properties of the turbulence, correlation length, dispersion relation and so on. The multichannel detection of the adjacent points in plasma allows us to measure the electric field, or the perpendicular plasma flow, directly by making a difference between potentials at two of the three channels.

The HIBP has a potential capability that has not been used so far except for a few examples;[32,33] e.g., the vector potential can be sensed from the beam movement. In CHS, we have explored this capability and have succeeded in measuring the magnetic field fluctuations directly (see Sec. VI) by making a difference between horizontal beam movements on the two channels. The details of the method are described in Ref. 27.

C. Plasma parameters for zonal flow experiments

The target plasmas for the zonal flow experiments have so far been produced with electron cyclotron resonance (ECR) heating of ~200 kW. The magnetic field strength of the discharges is $B=0.88$ T, and the density is kept constant approximately at $n_e \sim 5\times 10^{12}$ cm^{-3}. In this discharge condition, electron and ion temperatures, $T_e \sim 0.5$ keV and $T_i \sim 0.1$ keV (i.e., in collisionless regime), ion Larmor radius $\rho_i \sim 0.1$ cm, time scale of microinstabilities $\omega^*/2\pi \sim 50$ kHz with $k_\perp \rho_i \sim 0.3$, and energy confinement time $\tau_E \sim 2$ ms (or characteristic frequency of global confinement $\tau_E^{-1} \sim 0.1$ kHz), where $k_\perp$ is the wavenumber and ω^* is the drift frequency defined as $k_\perp T_e/eBL_n$ with L_n being a characteristic length of density gradient. The normalized plasma pressure (β-value) is ~0.2%.

III. ZONAL FLOW IDENTIFICATION

In order to prove the existence of zonal flows in toroidal plasmas, the first measurement of electric field fluctuation was carried out at the observation point of $r=12$ (or $\rho \sim 0.6$), which gives a maximum signal-to-noise ratio to the HIBP measurement. Figure 1(a) shows the spectrum of the measured electric field fluctuation. Note that the unit of the electric field position is expressed in volts, corresponding to the measured quantities; i.e., the potential difference between two channels. The actual value of the electric field can be obtained by dividing the potential difference by the sample volume distance estimated as $\Delta r \simeq 1$ cm.

In the measurements, it is confirmed that the low frequency fluctuation less than ~1 kHz shows a long-distance correlation. The waveforms of the fluctuations at two toroidal locations are quite identical with each other if the two

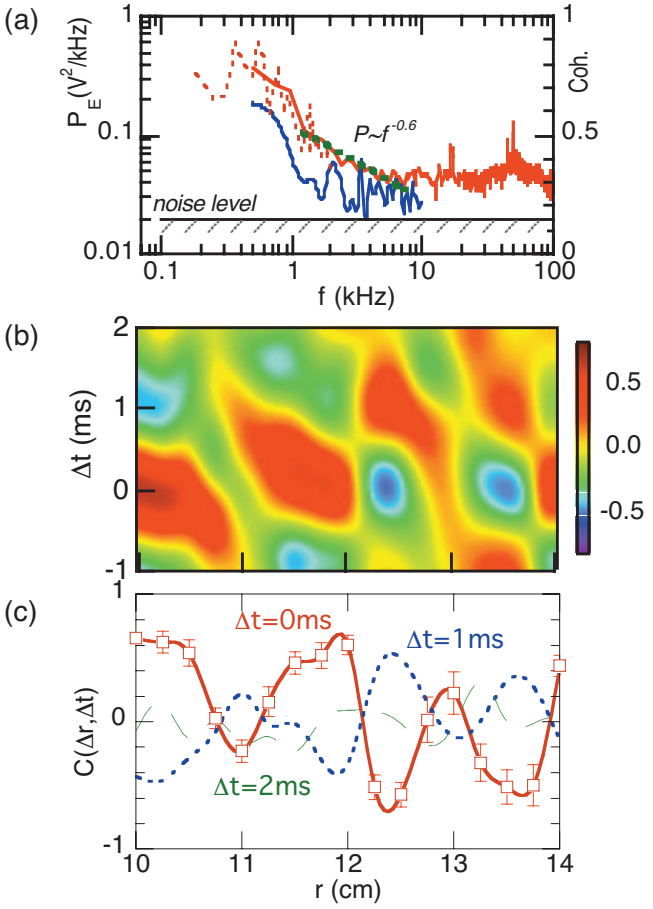

FIG. 1. (Color) (a) A power spectrum of potential difference at $\rho \sim 0.6$, and coherence between potential differences at the two toroidal locations. The electric field fluctuation ranging from 0.3 to 1 kHz shows long-distance correlation, and corresponds to the zonal flow of nearly zero frequency. The hatched region shows the noise level for the power density. (b) Spatio-temporal structure of stationary zonal flow evaluated from the correlation function in CHS. (c) Spatial correlations with the time lag of $\tau=0$, 1, and 2 ms (Ref. 10).

observation points are located on the same magnetic flux surface. On the other hand, the two observation points are located on different flux surfaces, the fluctuations are coherent with statistically almost an constant phase determined by the radial distance between the flux surfaces. This observation means that the fluctuation of this frequency is symmetric around the magnetic axis with a radial structure in mesoscale. Consequently, the fluctuations of this frequency are the stationary zonal flow. The fluctuation amplitude of this frequency range is approximately ~1 V; thus, the corresponding amplitude of the stationary zonal flow is 0.05–0.1 kV/m (or 0.06–0.11 km/s).

The detailed spatio-temporal structure of the stationary zonal flow can be inferred by altering the observed position of potential difference r_2, while fixing the other at r_1(=12 cm). The phase between electric fields at two locations can be deduced from traditional correlation coefficient and the fast Fourier transform (FFT) analysis of coherence and phase. The correlation between the potential differences, i.e., $C(\Delta r,\Delta t)=\langle \Delta\phi(r_2,t_2)\cdot\Delta\phi(r_1,t_1)\rangle/$

$\sqrt{\langle \Delta\phi(r_2,t_2)^2\rangle \cdot \langle \Delta\phi(r_1,t_1)^2\rangle}$, is evaluated, where $r_2=r_1+\Delta r$, $t_2=t_1+\Delta t$, and $\langle\psi\rangle=(1/2T)\int_{t-T}^{t+T}\psi dt$.

Figure 1(b) shows the correlation coefficient (closed circles) as a function of the radial distance of observation positions Δr. The plotted values are the ensemble averages of the correlation coefficients for time windows in stationary states. The correlation functions at several delay times are displayed in Fig. 1(c). The correlation function with $\Delta t=0$ shows a quasisinusoidal structure with a radial wavelength of $\sim$1.5 cm. The correlation function with $\Delta t=2$ ms shows no significant correlation, while the one with $\Delta t=1$ ms still indicates a high coherence keeping a quasisinusoidal structure. Accordingly, the radial wavelength of the stationary zonal flow is approximately $\sim$1.5 cm, while the lifetime of the zonal flow is $\sim$2 ms.

IV. NONLINEAR RELATIONSHIP BETWEEN ZONAL FLOWS AND TURBULENCE

A. Energy transfer between zonal flows and turbulence

The remaining issue for complete identification of the stationary zonal flow is to substantiate that the fluctuating *zonal structure* should be driven or coupled with the background turbulence. In order to establish the relation between turbulence and zonal flow, the observation is made in the interior of plasma at $\rho\sim0.35$, where the zonal flow amplitude is large. Figure 2(a) shows the spectrum of electric field fluctuation at that point, with coherence between electric field fluctuations at two toroidal positions. Compared with the spectrum in Fig. 1(a), the power of the stationary zonal flow is obviously larger in this case.

In order to investigate the relationship between zonal flow and the other fluctuations, the spectrum is divided into four regions: (i) zonal flow of $f<\sim1.5$ kHz, characterized by a quite high coherence of $\sim$0.7; (ii) an inertia region of $1.5<f<10$ kHz, called here a tail; (iii) the GAM region of $10<f<30$ kHz characterized by a sharp peak; and (iv) the background turbulence region with a broadband peak around $\sim$50 kHz. The sharp peak at 19 kHz shows a long-distance characteristic, or the significant coherence between the potential fluctuation at the two toroidal locations (>0.5). The peak is conjectured as the GAMs.

The relationships among the powers of these four frequency regions can be examined using a wavelet analysis. Figure 2(b) shows an example of the evolution of the zonal flow $Z(t)$ and that of the wavelet power spectrum of electric field fluctuation $W(f,t)$ at $\rho\sim0.35$. The used wavelet analysis[34] has the natural correspondence with the traditional Fourier transformation. The zonal flow component is filtered out from electric field fluctuation using a numerical low-pass filter (see details in Ref. 10). Note that the positive value means the ion diamagnetic direction. Although it is not shown in Fig. 2(b), significant correlations are seen between the temporal evolutions of zonal flow, turbulence, and tail in their power values.

In order to demonstrate the correlation between these three fluctuation regions, Fig. 2(c) shows three plots of normalized fluctuation power as a function of the normalized

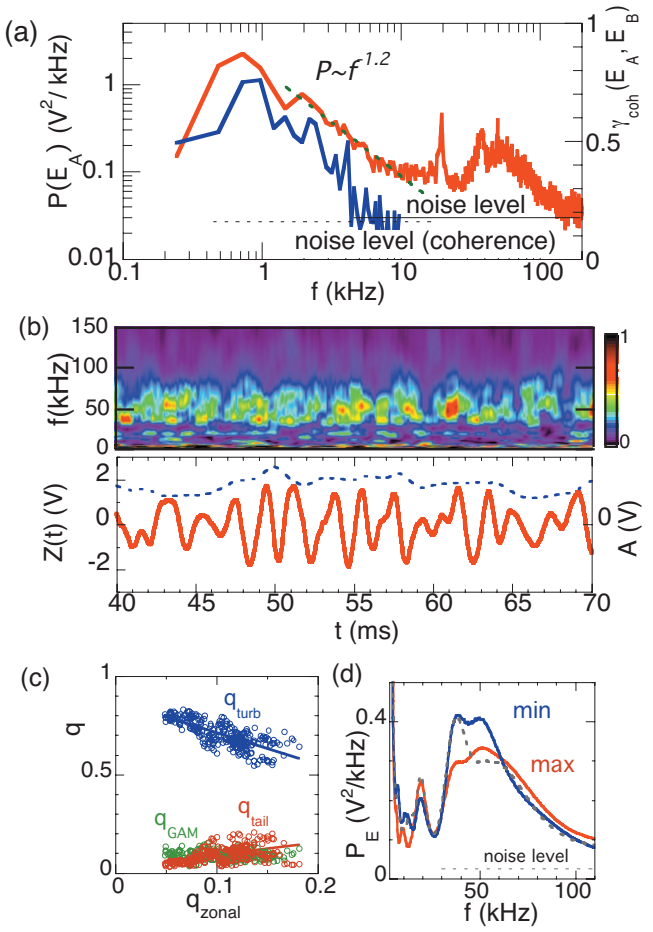

FIG. 2. (Color) (a) A spectrum of potential difference (or electric field) fluctuation. The measurement is carried out at $\rho\sim0.35$ (solid line). The coherence between electric field fluctuations at two toroidal locations (dashed line). The coherence is plotted in the low frequency range where the result is above the noise level. (b) Temporal evolution of wavelet spectrum of electric field fluctuations as a function of frequency, and that of zonal flow with low-pass filter. The unit of the color bar is in V^2/kHz. (c) Fluctuation power fractions in three frequency regimes as a function of that of zonal flow. (d) Conditional averaged spectra of wavelet power in the local maxima and minima of the zonal flow. The gray dashed line represents the conditional averaged spectrum when $|Z(t)|\sim0$ (Ref. 25).

zonal flow power, i.e., q_{zonal} [$=q(0.25,1.5\text{ kHz})$], where the normalized power is defined as $q(f_1,f_2)=\int_{f_1}^{f_2}W(f,t)df/W_{\text{total}}$, where W_{total} represents the wavelet power integrated all over the frequency. The regression analysis shows that the turbulence power $q_{\text{turb}}(30,200)$ should be strongly dependent on the zonal flow power as $q_{\text{turb}}\sim0.9-1.6q_{\text{zonal}}$ with their correlation coefficient being $\gamma=0.74$, while no significant relation $\gamma=-0.01$ is found for the fluctuation power of the coherent mode $q_{\text{GAM}}(10,30)$. On the other hand, the fluctuation neighboring to the zonal flow shows a positive correlation ($\gamma=0.49$), and follows the zonal flow concomitantly like a tail as $q_{\text{tail}}(1.5,10)\sim0.63q_{\text{zonal}}$. Accordingly, the zonal flow power fraction increases as the turbulence power fraction decreases,[25] suggesting that the quasienergy conservation law is valid between stationary zonal flow and turbulence.

In comparison between zonal flow and the wavelet fluctuation powers [Fig. 2(b)], the colored pattern seems to be synchronous with the tide of the zonal flow. In fact, the FFT

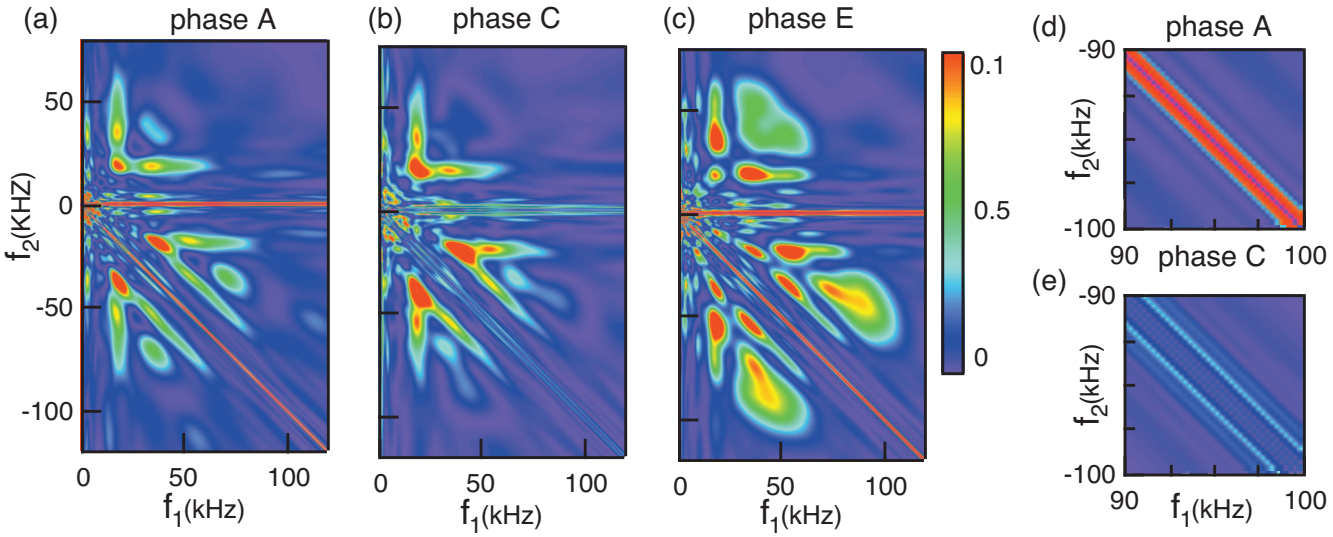

FIG. 3. (Color) Diagrams of wavelet squared bicoherence for three phases of zonal flow. The zonal flow is divided into five phases in its magnitude for the conditional integral of the wavelet bicoherence. Bicoherence diagram of (a) phase A (maximum), (b) phase C (zero), and (c) phase E (minimum). (d) An expanded view of the diagram for the phase A, and (e) that for the phase C (Ref. 26).

analysis indicates that the modulation frequency of turbulence power should coincide with the zonal flow frequency. The presence of the modulation can be examined by taking the conditional averages of the wavelet spectra for the phase of zonal flow. Figure 2(d) shows the conditional averaged wavelet spectra for the maxima and minima of the zonal flow. It is obvious that the fluctuation power around ~50 kHz shows an increase (an decrease) around a local minimum (a maximum) of the zonal flow. The result suggests that the fluctuation characteristics should be varied with the phase of flow, as well as with its amplitude.[24,25]

B. Quantification of couplings between flows and turbulence

Bicoherence analysis is used to quantify the strength of three wave couplings in a statistical and stationary manner.[29–31] As is shown in the previous subsection, the turbulence power is found to be modulated with the phase of flow; therefore, it can be expected that their coupling could be dependent on the phase of flow. The wavelet bicoherence analysis[34] should be an appropriate method to extract such intermittent linkage between the flow and turbulence.

The analysis is extended to adopt a conditional average for consideration of the dependence of the fluctuation properties on the flow phase.[26] The conditional bicoherence is evaluated on the electric field fluctuation for five phases of the flow [see Fig. 2(b)]: (A) $Z(\tau) > 0.8$ V, (B) $0.8 > Z(\tau) > 0.25$ V, (C) $0.25 > Z(\tau) > -0.25$ V, (D) $-0.25 > Z(\tau) > -0.8$ V, and (E) $Z(\tau) < -0.8$ V. The number of used ensembles is ~20 000 for every case.

Figure 3 shows three bicoherence diagrams for the phases A, C, and E. The results indicate clear changes in the coupling between component waves according to the phase of the flow. The most important feature is that higher bicoherence values are found along the lines of $f_1+f_2 \sim \pm 0.5$ kHz at the phases A (maximum) or E (minimum). The expanded views of a region ($90 < |f| < 100$ kHz) clearly demonstrate that the couplings becomes stronger on the lines of $f_1+f_2 \sim \pm 0.5$ kHz in the phase A, while the strong couplings on this line disappears in the phase C. This means that the background turbulence is intermittently coupled with the flow according to the phase of flow, suggesting that the modulational instabilities[3,35] should play an important role in the flow generation, as is expected from theories.

In addition, the couplings between turbulent waves are varied with the sign of the flow to cause the modulation of the turbulence power spectrum (Fig. 2). The corresponding increase can be seen particularly in the regions around $(f_1, f_2) \sim (50, -80)$ kHz, and $(f_1, f_2) \sim (80, -50)$ kHz in the bicoherence diagram of the phase E [Fig. 3(c)]. Besides, the coupling between GAMs (~20 kHz) and the background turbulence is also shown by the presence of the regions of higher bicoherence values around $f_1+f_2 \simeq \pm 20$ kHz, which does not show a significant dependence on the phase of the flow.

V. ROLE OF ZONAL FLOWS ON IMPROVED CONFINEMENT

Following the discovery of an internal transport barrier (ITB) in CHS,[36] similar phenomena have been found in various stellarators, despite the difference in their configurations.[37] The formation of the ITB was ascribed to the creation of a larger E_r shear between the two bifurcated branches of radial electric field; i.e., electron and ion roots.[38,39] In other words, the transition into the branch of strongly positive radial electric field forms the shear layer, whose radial width is 1–2 cm, in the boundary of the outside where the plasma still remains in the weakly positive branch of the radial electric field.

Actually, the fluctuation reduction in the connection layer has been confirmed just before and after the transition using twin HIBP measurements. Figure 4(a) shows an example of the fluctuation behavior on the barrier. In this case, one of the HIBP observes the change in the fluctuation at the

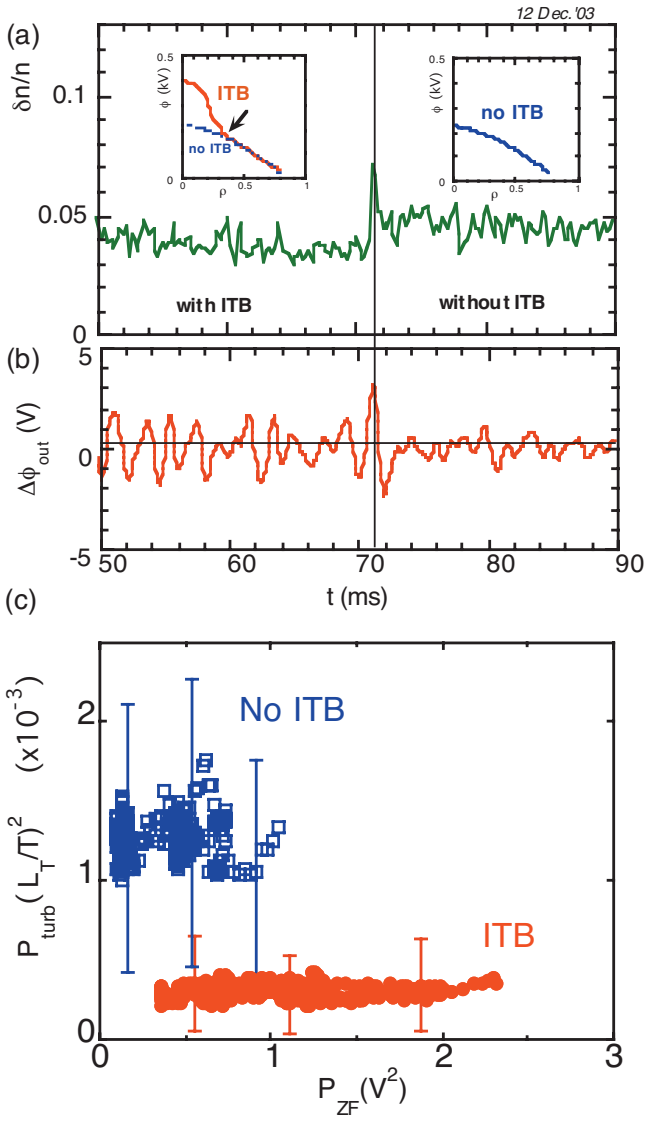

FIG. 4. (Color) (a) A change of density fluctuation amplitude and (b) a change in zonal flow amplitude before and after a transition. The potential profiles before and after the transition is shown in the insets. The solid vertical line indicates the transition time. The arrow in the left inset indicates the observation point of the fluctuations and zonal flow (Ref. 10). (c) Difference in energy partition between zonal flow and turbulence inside the barrier with and without a barrier. The turbulence is normalized by electron temperature gradient (Ref. 41).

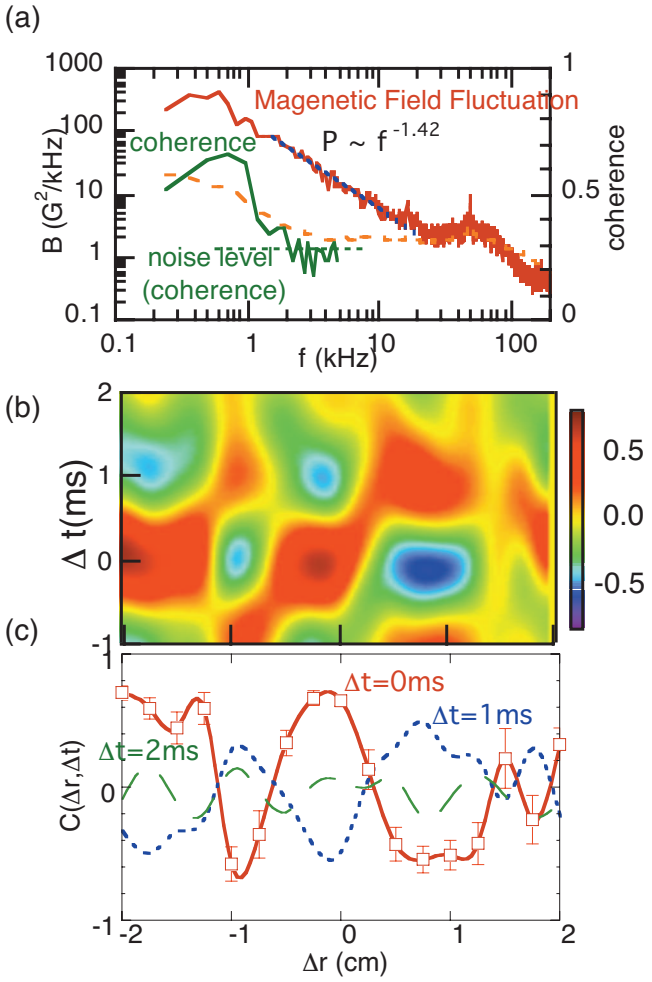

FIG. 5. (Color) (a) A power spectrum (poloidal component) and coherence between the magnetic field at two toroidal locations. The fluctuation less than ~1 kHz shows a quite high coherence, which means generation of global magnetic field of azimuthal symmetry. (b) Spatio-temporal correlation function $C(\Delta r, \Delta t)$ around the radial position of $r=12$ cm. (c) Correlation functions with three different time delays: $\Delta t=0$, 1, and 2 ms. These correlation diagrams show radial structure of zonal field, which has a quasisinusoidal radial structure with a characteristic radial wavelength (~1.5 cm) in mesoscale. On the other hand, the temporal correlation indicates that the memory of the mesoscale structure fades away with oscillation in ~2 ms (Ref. 28).

barrier location ($\rho \sim 0.3$), while the other is used as a monitor to indicate the exact time of the transition by sensing a discrete change in the potential inside the barrier ($\rho \sim 0.2$). As is shown in Figs. 4(a) and 4(b), the clear enhancement in the density fluctuation is observed just after the back transition of the radial electric field, together with a concomitant decrease in the flow amplitude.

On the other hand, it has been a mystery that the increase in the gradient of electron temperature inside the barrier location is larger than the neoclassical theory prediction, in spite of the absence of a significant change in radial electric field shear. The problem is solved by the recent observation of the energy partition between flow and turbulence. Figure 4(c) shows energy partition between flow and turbulence, demonstrating that a clear increase in the flow fraction should be the cause of the improvement in the state with the transport barrier.[41] Note that the turbulence power is normalized by the temperature gradient in order to remove the effect of the change of the driving force before and after the transition.

The improvement inside the barrier should be interpreted as the result that the free energy of the increased pressure inhomogeneity should be preferentially transferred into the flow energy in that state with the transport barrier. The preferential energy transfer to the flow should be ascribed to the effective viscosity reduction in the state of the electron root. Since the equation of the radial current balance is expressed as $\delta j_{\mathrm{turb}} + (\partial j_{r,\mathrm{neo}}/\partial E_r)\delta E_r = 0$, where δj_{turb} means the turbulence induced current to drive the flow (radial electric field), the neoclassical driven current $(\partial j_r/\partial E_r)$ acts as the effective viscosity. Both the neoclassical theories and the experimental observations indicate that the effective viscosity $(\partial j_r/\partial E_r)$ is

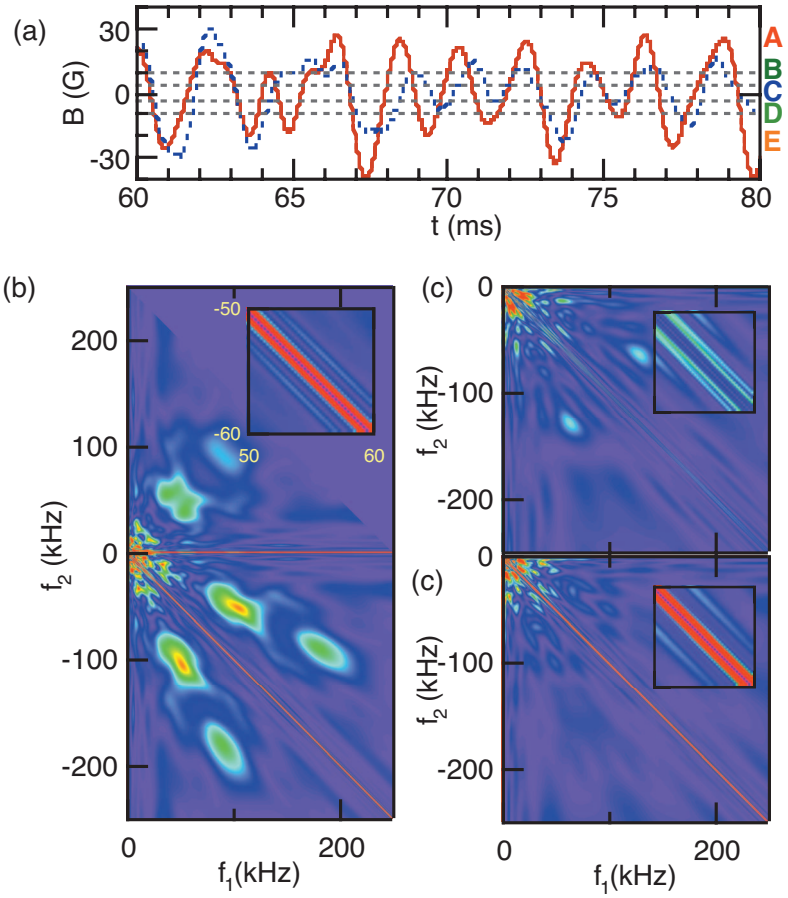

FIG. 6. (Color) (a) The waveforms of zonal fields at the same radial but different toroidal locations. Bicoherence diagrams of (b) phase A, (c) phase C, and (d) phase E. The insets are expanded views of a frequency range of $50<f_1<60$ kHz and $-60<f_2<-50$ kHz (Ref. 28).

smaller in the electron root than in the ion root.[40] Therefore, the improved confinement inside the barrier should be realized by the increase of the flow fraction due to the reduction of the flow damping rate in the state of electron root.

VI. IDENTIFICATION OF ZONAL MAGNETIC FIELD

Several theories have been proposed to predict the existence of magnetic field in toroidal plasmas.[3,42,43] In order to confirm the existence of such structured magnetic field generated by turbulence, the measurement of magnetic field fluctuation using the newly developed technique for HIBP was carried out at the radial position of $r_{\mathrm{obs}}\sim 12$ cm (or $\rho\sim 0.6$), where the maximum signal-to-noise ratio was obtained for the HIBPs in the ECR-heated plasmas. A trajectory calculation shows that the horizontal beam movement reflects the poloidal magnetic field in this series of measurement.[27]

Figure 5(a) shows the measured spectrum of the magnetic field fluctuation, together with coherence between two toroidal locations. The dashed line is the estimated maximum (or the upper boundary) of contamination due to the electric field fluctuation. The coherence of the frequency lower than 1 kHz, where the contamination is sufficiently small, is quite high (~0.7). As is similar to the case of the flow, the detailed investigation shows that the magnetic field fluctuations of this frequency are identical at two toroidal positions if they are on the same magnetic field surface. On the other hand, it has been also confirmed that two signals on slightly different magnetic flux surfaces are coherent with statistically almost a constant phase as zonal flows. Consequently, the fluctuation less than ~1 kHz should have symmetric structure around the magnetic field axis with a radial structure in mesoscale.[28]

A constant phase relation between the signals from two different radial positions allows us to estimate the spatio-temporal characteristics of the zonal magnetic field in the radial direction by evaluating the correlation function, $C(\Delta t,\Delta r)$ in exactly the same manner as that of the zonal flow. Figure 5(b) shows the cross-correlation obtained by altering an observed position r_2, shot by shot with fixing the other at r(=12 cm). Figure 5(c) illustrates the spatial structure of three times at $\Delta t=0,1$ and 2 ms. These correlation diagrams show a quasisinusoidal structure in the radial direction with a characteristic radial wavelength of $\lambda_r\sim 1.5$ cm, while the memory of the structure is lost in ~2 ms.

The wavelet bicoherence analysis is applied to prove the causal relationship between the zonal magnetic field and turbulence for the five phases of the zonal magnetic field. Figure 6 shows some of the obtained bicoherence diagrams using a conditional average for the five phases of zonal magnetic field [see Fig. 6(a)]: (A) $B_Z>10$ G, (B) $10>B_Z>3$ G, (C) $|B_Z|<3$ G, (D) $-3>B_Z>-10$ G, and (E) $B_Z<-10$ G. Two bright lines $f_1+f_2=\pm 0.5$ kHz in the bicoherence diagrams for phases A and E [Figs. 6(b) and 6(d)] clearly demonstrate that nonlinear couplings between turbulence fluctuation and zonal magnetic field increases when the

zonal magnetic field stays near the maxima and the minima. On the other hand, no significant coupling is seen in phase C [Fig. 6(c)]. Consequently, the wavelet bicoherence analysis verifies the existence of the coupling between zonal magnetic field and turbulence and its intermittent behavior associated with the zonal magnetic field phase, suggesting that the modulational instabilities should play an important role in the field generation, as is similar to the case of zonal flow.

VII. DISCUSSION AND SUMMARY

A series of CHS experiments on zonal flows and turbulence have unambiguously demonstrated the existence of zonal flows, a mesoscale structure, that are nonlinearly driven by the background turbulence. Consequently, the plasma turbulence should be regarded as a system of drift waves and zonal flows that nonlinearly interact with each other. The discovery provides a new paradigm to deal with plasma turbulence and the resultant transport. The new paradigm indicates that the importance of disparate scale interactions among micro-, macro-, and mesoscale structures may be a key to resolve several mysterious problems in toroidal plasmas, such as nonlocal transport. Actually, the energy partition between zonal flows and turbulence gives an answer to solve the transport improvement inside the barrier in CHS, where no significant shear exists.

On the other hand, turbulence-generated structure should be ubiquitously observed in the universe; therefore, the study of structural formation in CHS gives a deep insight into such phenomena. The present experimental results demonstrate that the physics of zonal flows, in fact, is equivalent to that of rotating star atmosphere, like the Jovian zonal flows, as was pointed out already. It should be emphasized that the discovery of zonal magnetic field should be the first experimental evidence that turbulence should really generate a structured magnetic field, consequently, should be a great step for solving a historical physical problem; i.e., dynamo-dipole magnetic field generation in rotating stars.

In summary, the experiments of zonal flow and turbulence using HIBPs in CHS clearly demonstrates that a medium size toroidal plasma is quite beneficial for physical understanding of the structural formation of turbulent plasma ubiquitously observed in the universe. The laboratory experiments on turbulence and zonal flows should be very important not only for the fusion science but also for astrophysics; more generally, for understanding the structural formation associated with turbulence.

ACKNOWLEDGMENTS

This work is partly supported by the Grant-in-Aids for Scientific Research (No. 15360497) and Specially-Promoted Research (No. 16002005). The authors are grateful to Professor O. Motojima for his continuous support and encouragement.

[1] G. P. Williams, J. Atmos. Sci. **35**, 1399 (1978).
[2] A. Hasegawa, C. G. Maclennman, and Y. Kodama, Phys. Fluids **22**, 2122 (1979).
[3] P. H. Diamond, K. Itoh, S.-I. Itoh, and T. S. Hahm, Plasma Phys. Controlled Fusion **47**, R35 (2005).
[4] A. Hasegawa and M. Wakatani, Phys. Rev. Lett. **59**, 1581 (1987).
[5] M. N. Rosenbluth and F. L. Hinton, Phys. Rev. Lett. **80**, 724 (1998).
[6] Z. Lin, T. S. Hahm, W. W. Lee, W. M. Tang, and R. B. White, Science **281**, 1835 (1998).
[7] P. H. Diamond and S. Champeaux *et al.*, Nucl. Fusion **41**, 1067 (2001).
[8] K. Hallatschek and D. Biskamp, Phys. Rev. Lett. **86**, 1223 (2001).
[9] A. M. Dimits, G. Bateman, M. A. Beer, B. I. Cohen, W. Dorland, G. W. Hammett, C. Kim, J. E. Kinsey, M. Kotschenreuther, A. H. Kritz, L. L. Lao, J. Mandrekas, W. M. Nevins, S. E. Parker, A. J. Redd, D. E. Shumaker, R. Sydora, and J. Weiland, Phys. Plasmas **7**, 969 (2000).
[10] A. Fujisawa, K. Itoh, H. Iguchi *et al.*, Phys. Rev. Lett. **93**, 165002 (2004).
[11] G. R. Tynan, C. Holland, J. H. Yu, A. James, D. Nishijima, M. Shimada, and N. Taheri, Plasma Phys. Controlled Fusion **48**, S51 (2006).
[12] G. S. Xu, B. N. Wan, M. Song, and J. Li, Phys. Rev. Lett. **91**, 125001 (2003).
[13] D. K. Gupta, R. J. Fonck, G. R. McKee, D. J. Schlossberg, and M. W. Shafer, Phys. Rev. Lett. **97**, 125002 (2006).
[14] M. Jakubowski, R. J. Fonck, and G. R. McKee, Phys. Rev. Lett. **89**, 265003 (2002).
[15] M. G. Shats and W. M. Solomon, Phys. Rev. Lett. **88**, 045001 (2002).
[16] Y. Hamada, A. Nishizawa, T. Ido, T. Watari, M. Kojima, Y. Kawasumi, K. Narihara, K. Toi, and JIPPT-IIU Group, Nucl. Fusion **45**, 81 (2005).
[17] T. Ido, Y. Miura, K. Hoshino *et al.*, Nucl. Fusion **46**, 512 (2006).
[18] G. R. Mckee, R. J. Fonck, M. Jakubowski, K. H. Burrell, K. Hallatschek, R. A. Moyer, W. Nevins, D. L. Rudakov, and X. Xu, Plasma Phys. Controlled Fusion **45**, A477 (2003).
[19] G. D. Conway, B. Scott, J. Schirmer, M. Reich, A. Kendl, and the ASDEX Upgrade Team, Plasma Phys. Controlled Fusion **47**, 1165 (2005).
[20] P. M. Schoch, K. A. Connor, D. R. Demers, and X. Zhang, Rev. Sci. Instrum. **74**, 1846 (2003).
[21] A. Fujisawa, K. Itoh, A. Shimizu, H. Nakano, S. Ohshima, H. Iguchi, K. Matsuoka, S. Okamura, S.-I. Itoh, and P. H. Diamond, Plasma Phys. Controlled Fusion **48**, S31 (2006).
[22] A. Krämer-Flecken, S. Soldatov, H. R. Koslowski, O. Zimmermann, and TEXTOR team, Phys. Rev. Lett. **97**, 045006 (2006).
[23] A. Fujisawa, T. Ido, A. Shimizu *et al.*, Nucl. Fusion **47**, S718 (2007).
[24] A. Fujisawa, A. Shimizu, H. Nakano *et al.*, Plasma Phys. Controlled Fusion **48**, S205 (2006).
[25] A. Fujisawa, A. Shimizu, H. Nakano *et al.*, J. Phys. Soc. Jpn. **76**, 033501 (2007).
[26] A. Fujisawa, A. Shimizu, H. Nakano *et al.*, Plasma Phys. Controlled Fusion **49**, 211 (2007).
[27] A. Fujisawa, A. Shimizu, H. Nakano, and S. Ohshima, Plasma Phys. Controlled Fusion **49**, 845 (2007).
[28] A. Fujisawa, K. Itoh, A. Shimizu *et al.*, Phys. Rev. Lett. **98**, 165001 (2007).
[29] Y. C. Kim and E. J. Powers, IEEE Trans. Plasma Sci. **PS-7**, 120 (1979).
[30] D. Brésillon and M. S. Hohamed-Benkadda, Phys. Fluids **31**, 1904 (1988).
[31] Y. Nagashima, K. Hoshino, A. Ejiri *et al.*, Phys. Rev. Lett. **95**, 095002 (2005).
[32] T. P. Crowley, IEEE Trans. Plasma Sci. **22**, 291 (1994).
[33] V. J. Simicic, K. A. Connor, T. P. Crowley, R. L. Hickok, P. M. Schoch, A. J. Wootton, X. Z. Yang, and Y. Z. Zhang, Rev. Sci. Instrum. **61**, 3061 (1990).
[34] B. Ph. Van Milligen, C. Hidalgo, and E. Sanchez, Phys. Rev. Lett. **74**, 395 (1995).
[35] L. Chen, Z. Lin, and R. B. White, Phys. Plasmas **7**, 3129 (2000).
[36] A. Fujisawa, H. Iguchi, T. Minami *et al.*, Phys. Rev. Lett. **82**, 2669 (1999).
[37] A. Fujisawa, Plasma Phys. Controlled Fusion **45**, R1 (2003).
[38] L. M. Kovrizhnykh, Nucl. Fusion **24**, 435 (1984).
[39] D. E. Hastings, W. A. Houlberg, and K. C. Shaing, Nucl. Fusion **25**, 445 (1984).
[40] A. Fujisawa, H. Iguchi, K. Itoh *et al.*, Phys. Rev. Lett. **79**, 1054 (1997).
[41] K. Itoh, S. Toda, A. Fujisawa, S.-I. Itoh, M. Yagi, A. Fukuyama, P. H. Diamond, and K. Ida, Phys. Plasmas **14**, 020702 (2007).
[42] I. Gruzinov, A. Das, P. H. Diamond, and A. Smolyakov, Phys. Lett. A **302**, 119 (2002).
[43] P. N. Guzdar, R. G. Kleva, A. Das, and P. K. Kaw, Phys. Rev. Lett. **87**, 015001 (2001).